History of long-term glacial erosion in the Patagonian Andes

Chelsea Willett

Advisor: Mark Brandon

Second Reader: David Evans

April 27, 2011

A Senior Thesis presented to the faculty of the Department of Geology and Geophysics, Yale University, in partial fulfillment of the Bachelor's Degree.

In presenting this thesis in partial fulfillment of the Bachelor's of Science Degree from the Department of Geology and Geophysics, Yale University, I agree that the department may make copies or post it on the department website. I further agree that extensive copying of this thesis is allowable only for scholarly purposes. It is understood, however, that any copying or publication of this thesis for commercial purposes of financial gain shall not be allowed without my written consent.

Chelsea D. Willett
27 April 2011

Abstract

In the Patagonian Andes, home to the third largest ice field in the modern world, we investigate the influence of erosion via the glacial buzz saw on the mountain belt since its initial uplift ~25-20 Ma. It is thought that extensive glaciation began in the area 6 Ma or earlier. Plio-Pleistocene cooling sets up a natural experiment in Patagonia: was topography rapidly removed to establish the modern correlation between glacier extent and maximum elevations in only a few million years, or was this correlation developed on a longer timescale, implying that alpine glaciers were important erosive agents prior to the Pliocene? In the former case a major increase in erosion rates coincident with cooling would be expected, in the latter case, erosion rates would remain fairly steady from Pliocene to present. The eastern flank of Patagonia features a unique sequence of well-dated moraines and tills, each containing granitic cobbles derived from the Patagonian Batholith. Mean (U-Th)/He apatite cooling (AHe) ages from these deposits yield a record of the average erosion rate in the high Andes over time. Preliminary results suggest that erosion rates have accelerated over the past 20 Ma, from as slow as 0.1 mm yr^{-1} to 0.45 mm yr^{-1}. Additionally, LGM ice models predict that the ice divide sat west enough to transport material from the Jurassic-Cretaceous granite pluton on the west side of the mountain belt to the east to form the glacial deposits seen today. These results support the global cooling concept and indicate that rock transport crossed the modern continental divide, further developing a long-term erosional history of the area.

Introduction

Glaciers are known to have a high erosion capacity: the sliding base of a glacier can erode as much as 1 m of bedrock material for every 1 km of sliding (Hallet et al., 1996). Glaciers can also be frozen based, where the ice/bedrock interface involves no sliding so erosion is minimal. Being a sliding base or frozen base glacier is determined by glacier thickness and ambient temperatures.

It is the highly erosive, sliding base glaciers that are thought to play a key role in shaping topography. These sliding base glaciers are found on mountains, at latitudes where the average yearly temperatures are low enough, but also at lower latitudes, at altitudes where the atmospheric lapse rate makes ambient temperature sufficiently low for enough of the year. Possible glacier localities are further limited by the constraint that, in order to build a glacier, sufficient precipitation is needed.

This configuration presents an interesting question: as a mountain belt grows, it rises to create an ideal location for glaciers, but the glaciers in turn erode the mountain belt. We strive to understand where this relationship balances, a theory called the “glacial buzz saw,” the idea that equilibrium line elevations (ELAs, or snowlines) control the maximum height of peaks (Reiners and Brandon, 2006). Glacier ELA is a contour that defines the meeting line of the zones of ablation and accumulation.

It has long been assumed that the glacier ELA controls the height of the Andes (Fig. 1). Note the transition from fast to slow erosion rates around 48ºS, likely due to a transition from sliding- to frozen-base glaciers.

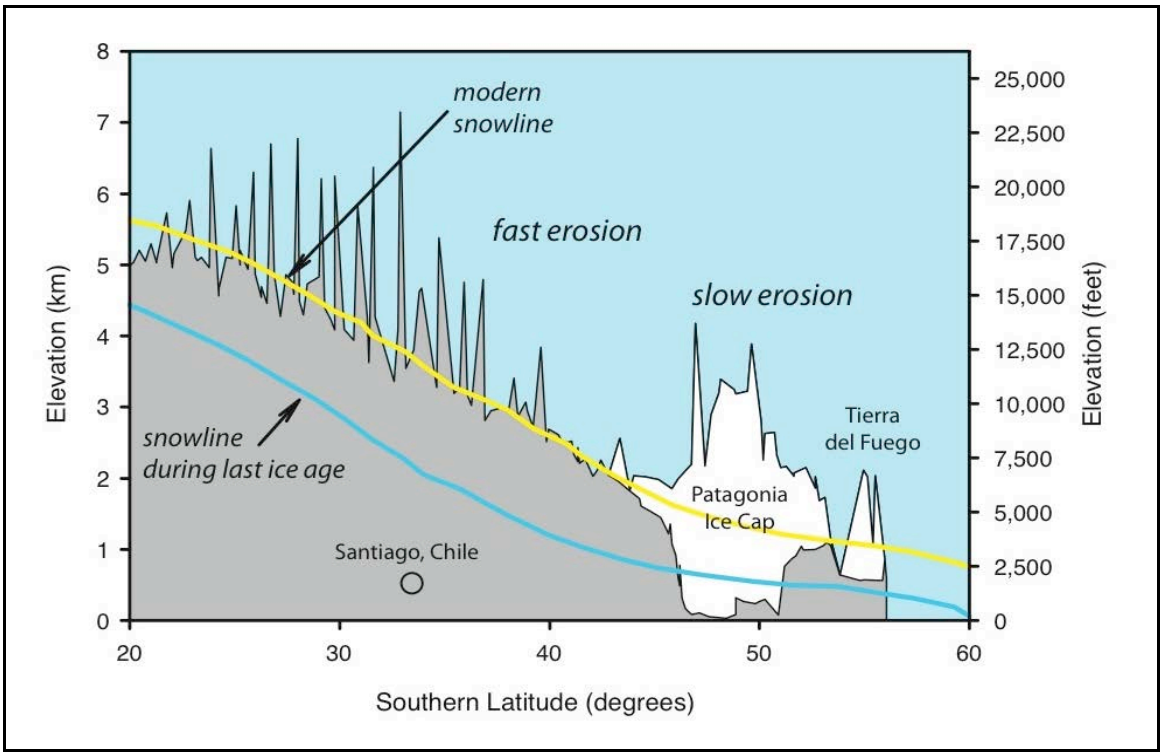

Figure 1: Variation in expected erosion rates in the Andes relative to past and present ELA (snowline). Between ~20ºS and 45ºS, fast erosion occurs, matching the modern snowline to the modern topography. South of 48ºS, glaciers transition to frozen base, decreasing the erosion rate (by Steve Porter, as presented in Broecker and Denton, 1990).

Is the assumption that ELA controls the Andes valid? My contribution to this investigation is to search for evidence of the glacial buzz saw in the Andes. The Andes present a natural experiment for answering this question. Initial uplift began at about 25 Ma to 20 Ma (Gregory-Wodzicki, 2000) and extensive glaciation began in the area at or earlier than 6 Ma (Thomson et al., 2010). They run a north-south transect of the Southern Hemisphere, crossing latitudes from nearly 10ºN down to 55ºS (Fig. 2). Between 35ºS and 55ºS, the study area for this project, virtually all of the region's precipitation – 2 to 4 m yr^{-1} – falls on the western flank of the mountain belt, creating and maintaining large glaciers (Montgomery et al., 2001). The land to the east is in the Andes rain shadow and

is dry, thereby better preserving the glacial deposits, both moraines and tills. The final feature of the Andes is the fortuitous presence of magmatism throughout the Pliocene and Pleistocene, which brackets the glacial deposits between planar, datable layers.

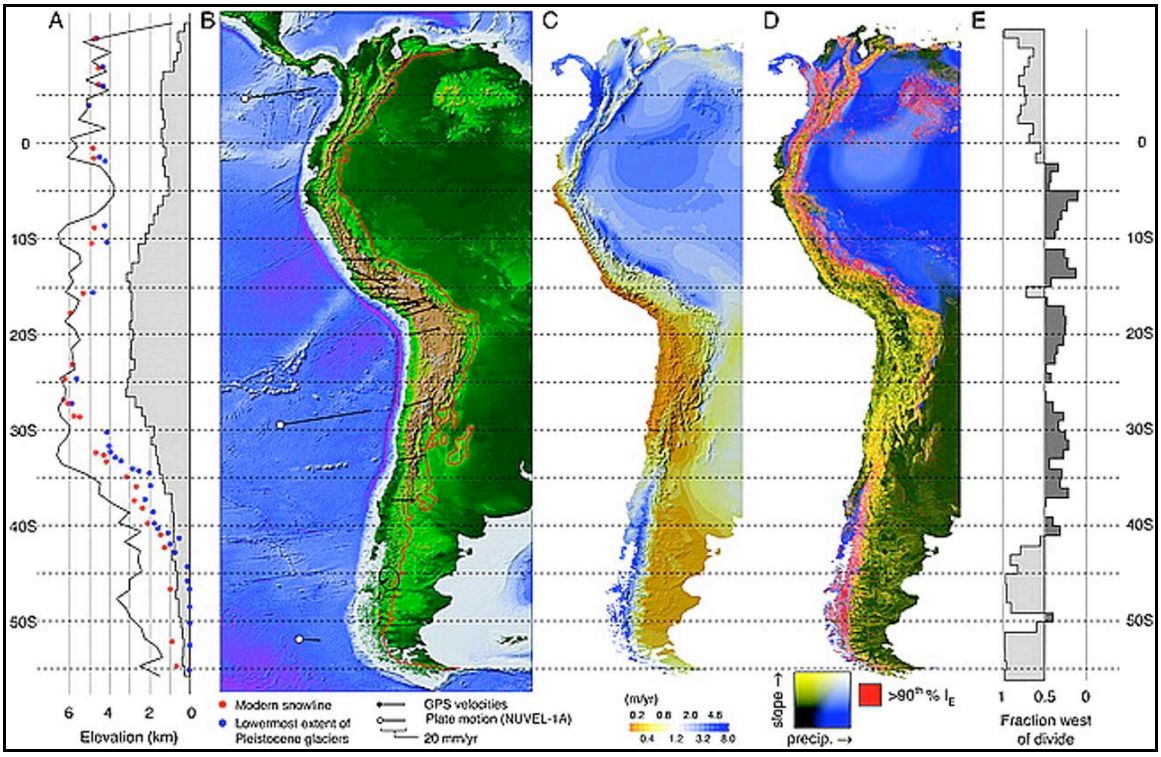

Figure 2: This figure shows the latitudes spanned by the Andes in South America. (a) Maximum and mean elevation (thin line and gray area, respectively) for each degree latitude as well as modern snowline and Pleistocene low elevation. (b) Topography and bathymetry of western South America and the eastern Pacific Ocean. (c) Mean annual precipitation on a relief map of western South America (from Montgomery et al., 2001. See references for access to higher-resolution image)

I use thermochronometric dating to estimate paleo-erosion rates and better understand the surface processes that sculpted the landscape long ago. What moved where? How?

We observe that the moraines that lie east of the Andes contain 5-10% granite cobbles. The nearest source for these rocks is the Patagonian batholith,

which makes up the core of the Andes. The cobbles show evidence of being transported by glaciers, such as roundedness or striations in some cases. The batholith and the ice fields lie entirely west of the continental divide so mass transport between the western and eastern flanks is minimal. There is no modern feasible way for the granite to get from the source region to the deposit, that is, from the west side to the east side. This cannot always have been the case. The presence of these cobbles to the east tells us that the ancient Andes were different from the Andes of today.

The goal of this project is to reconstruct the landscape of the Patagonian Andes and understand the role that glaciation has played in defining mountain topography and mass transport in the region. This investigation involves observing the relative positions of the ice divide and the continental divide through the Last Glacial Maximum (LGM) and Greatest Patagonian Glaciation (GPG), measuring the cooling ages of batholith-sourced granites and calculating the paleo-erosion rates associated with the Patagonian Andes.

Study Area

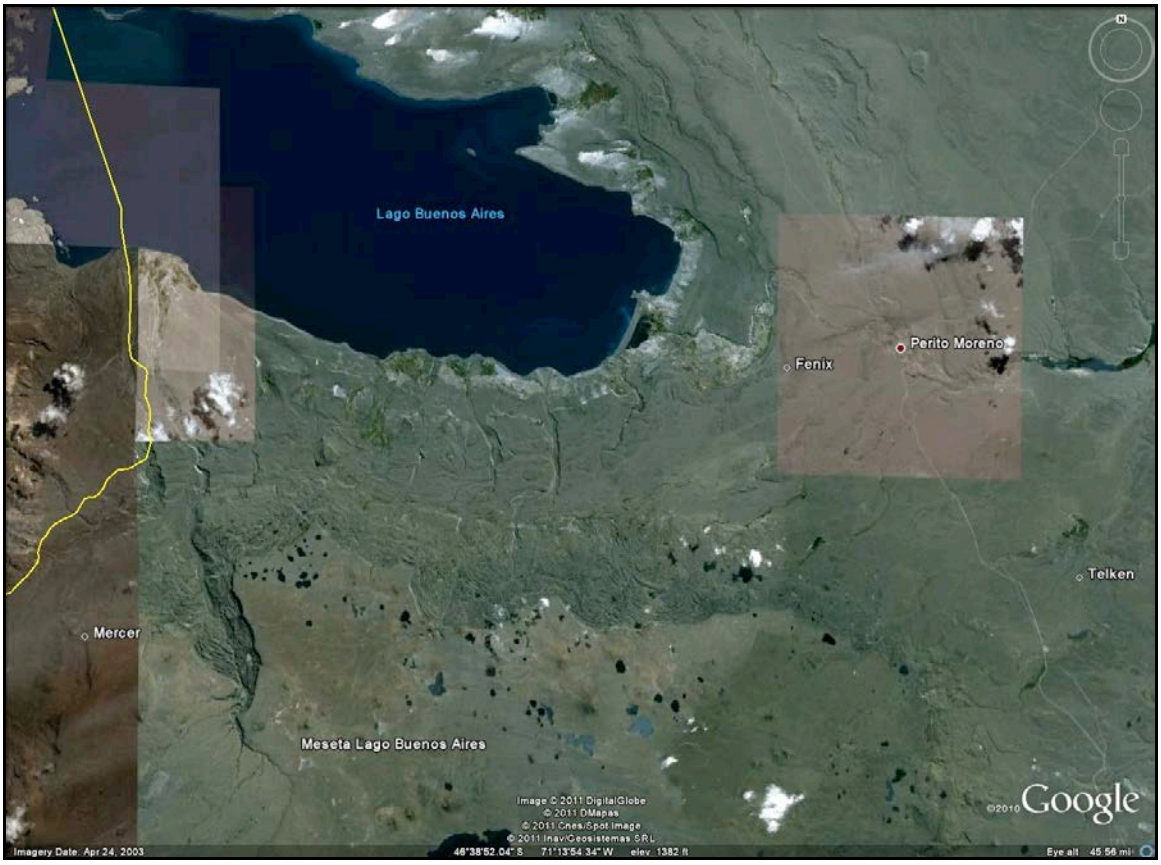

Figure 3: The moraines relative to Lago Buenos Aires. Samples presented at this stage of the research were collected from Fenix I, Telken, and the Mercer. Created by C. Willett using Google Earth. See appendix images A3-A5 for photographs of the three sampling sites.

The southern Andes present a series of glacial moraines and tills interspersed with extrusive igneous basalts. The study area is to the east and south of General Carrera-Lago Buenos Aires (LBA) and contains the Meseta Lago Buenos Aires, from roughly 45°S to 48°S and 70°W to 73°W (Fig. 3). This location is also due east of a tectonic triple junction, a divergent plate boundary that is being subducted beneath a third plate. The subduction of this plate boundary is thought to bring about the magmatism of the region (Lagabrielle et al, 2010).

Cycles of glaciation and deglaciation are interspersed with basaltic eruptions that create datable, planar boundaries that bracket the glacial deposits. Previous studies have successfully dated a number of these flows, which jumpstarts this project by giving a time of deposition (Kaplan et al., 2004; Singer et al, 2004; Mercer and Sutter, 1982). Knowing the time of deposition is one if the key components in calculating lag time, described in Methods.

Additionally, the simple geology of this portion of the Andes makes it easier to determine when and where transport took place. The Patagonian batholith, which makes up the ridge crest and western flank of the Andes in the study area, is the only source of granitic rocks in the region. The tills and moraines in the study area contain granite cobbles as well as regionally metamorphosed rock associated with the batholith.

Methods

Four main techniques were used in the reconstruction of the Patagonian Andes: digitizing and mapping ice extent, calculating flow lines, measuring age, and calculating paleo-erosion rates.

I. Mapping Ice Extent

In order to understand the relative positioning of the modern continental divide, which is the Chile-Argentina border north of 52°S, I studied Hulton's ice model, which estimates ice extent and thickness in all of Patagonia at the Last Glacial Maximum (LGM), 19,000-23,000 years ago.

Using Didger 4, I georeferenced the Hulton image to a reference map of South America, created with the General Mapping Tool (GTM) in Universal Transverse Mercator (UTM WGS 84). Ten points of reference were used for an accurate fit. In a new layer, I traced each 250-m ice elevation contour using a polyline and assigned the elevation value in meters as the primary polyline attribute. This new layer of the digitized, georeferenced ice sheet was then saved as a shapefile and exported to ArcMap 10.

Within ArcMap, the shape files were added to a 2-D geologic map of the research area. Creation of an interpolated 3-D ice surface is in progress. Incorporating these surfaces into modern 2-D and 3-D maps of the region answers two questions: *if* and *when*. First, it allows us to determine if the ice sheet was ever large enough and positioned properly to move material over and east of the modern continental divide. Second, it gives a time period in which transport from the batholith on the western side to the glacial deposits on the eastern side of the continental divide could occur.

II. Calculating Ice Flow

To estimate the flow of ice in the ice sheet, I exported the contour lines from Methods I as a shapefile from Didger and imported it into Matlab, I then aided Dr. Brandon as he completed the bulk of the following steps. First, all the contour lines were converted into points with elevation as an attribute for each. Second, we set up a set of points along the perimeter of the grid that were lower (-1 m) than all of the existing points. The next step was to grid all the data. With

that in hand, we made a set of points evenly distributed along the ice sheet outline (the mask contour). With this completed dataset, we simply calculated streamlines, a Matlab command that calculates lines that follow the maximum gradient at each point, creating a path of steepest descent. These lines were the plotted with the mask contour and the whole shape placed over a map of southern South America in ArcMap (Fig. 8).

III. Measuring Age

The (U-Th)/He method of dating apatite-containing rocks, like the granite of the Patagonian Batholith, is based on the accumulation of ^{4}He produced by the α-decay of the parent ^{238}U, ^{235}U, and ^{232}Th isotopes. Radiogenic ^{4}He readily diffuses out of the apatite until it cools to ~70ºC, after which diffusion essentially stops. The concentration of ^{4}He and the parent isotopes can be used to calculate a cooling age. Measurements are by first degassing of the crystal by heating and gas-source mass spectrometry to measure ^{4}He, followed by inductively-coupled plasma mass spectrometry on the same crystal to measure U and Th (Reiners and Brandon, 2006).

Because the relation between temperature and depth is well understood below the earth's surface, the cooling age offers an insight into how far below the surface the diffusion of ^{4}He stopped and the clock started. Assuming a simple exhumation path, this length scale and time scale can be used to estimate a time-averaged erosion rate for the apatite-containing rock (Fig. 4).

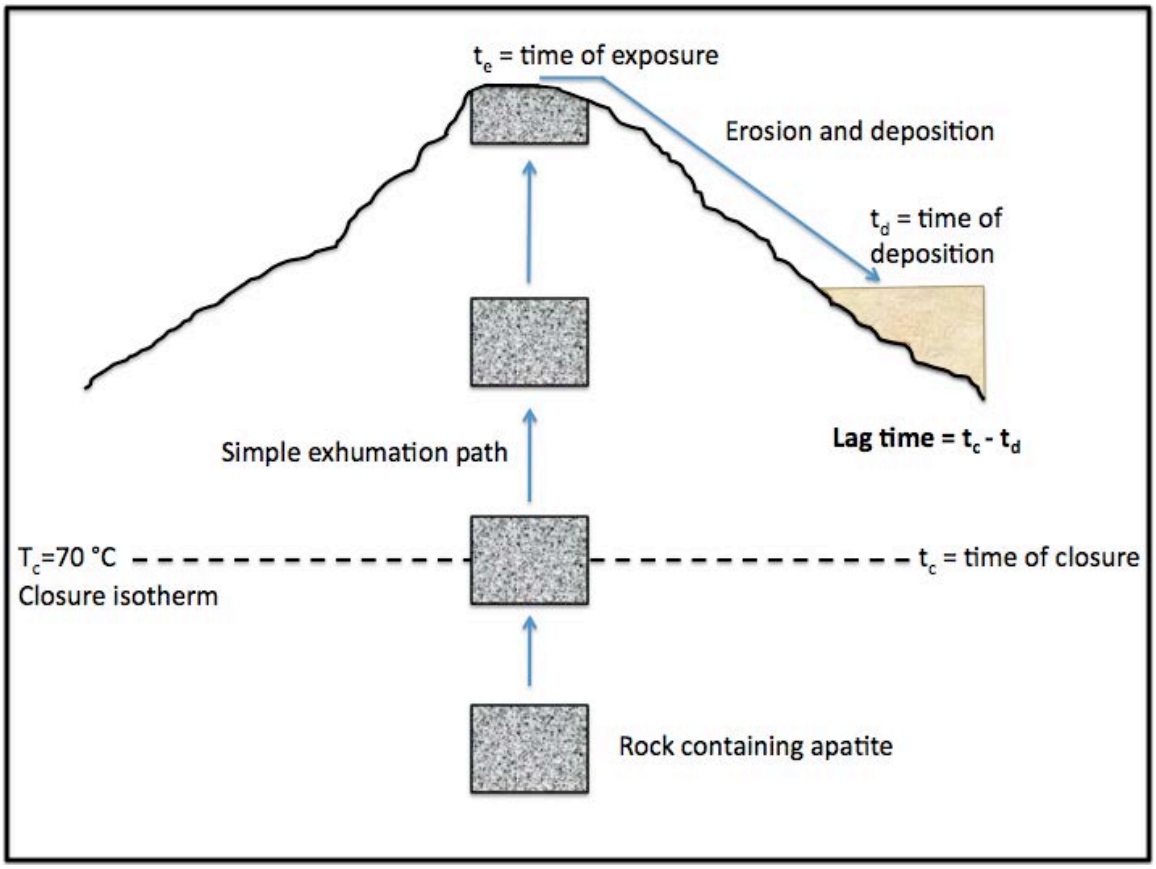

Figure 4: Apatite-containing rock cools below its closure temperature (T_c , range of a few degrees because of Partial Retention Zone (see Reiners and Brandon 2006)) at time t_c as it is exhumed to the surface. Once at the surface, at time t_e, cobbles are picked up by glaciers and ice sheets and deposited at time t_d. Lag time simply integrates between t_c and t_d and mainly represents the exhumation time (C. Willett, after Bernet et al, 2009).

Samples were collected from three glacial deposits near Lago Buenos Aires in Provincia Santa Cruz, Argentina. Cobbles were selected from these deposits because each has bracketing basalt flows that have been dated. The deposits are: the Fenix I moraine, deposited during the Last Glacial Maximum at 15.6±1.1 ka (Kaplan et al., 2004); Telken moraine, with a depositional age of 760±14 to 984±35 ka (Singer et al, 2004); and the oldest preserved till, here called Mercer, with a depositional age of 7 to 5 Ma (Mercer and Sutter, 1982). These three sampling sites are shown on a map of the region in Figure 3.

We employ a method wherein we date multiple granite cobbles from one source region to establish tighter bounds on the igneous rock source area. Each granite cobble weighed 6 to 10 pounds. In the rock lab at Yale University, cobbles were coarsely crushed on a BICO Chipmunk Crusher, finely ground on a disc mill (BICO Braun Pulverizer, type UA), and sieved on a 32-mesh of 500 microns using a Ro-Tap. Samples were then bagged and shipped to the University of California Santa Cruz where Keith Ma and I completed the mineral separations. First, the samples were separated by density on a shaker table, which separates the densest roughly 20% of the sample from the rest. After an overnight soak in hydrogen peroxide, samples were dried in a 40ºC oven and prepared for magnetic separation on the Franz Isodynamic Separator.

The magnet of the Franz was flipped vertically in order to do a rough separation of strongly magnetic grains from the rest of the sample using a stepped set of magnetic fields, defined by currents. The two sets were [0.5 A, 1.0 A, 1.5 A and 2.0 A] or and [0.5 A and 2.0 A]. The remaining non-magnetic portion of the sample, about 200 g, was put through a separation funnel of lithium metatungstate (LMT), specific gravity of 3.7, separating the heavier apatites and zircons from the other lighter minerals. After drying off the LMT in the 40ºC oven, samples were put through the Franz once more. In this case, the Franz is used in its standard configuration (at a tilt with a vibrating, metal slide) to remove any trace magnetic material.

The end sample, less than a thimbleful of material, was then picked on a microscope for apatite crystals. Apatites of >60 microns across and minimal

inclusions were selected for dating. Not all samples contained ideal apatite grains, so in many cases, broken grains or grains with minor inclusions were selected. In the data processing, a correction factor is applied to these broken crystals. See Appendix for images of selected apatite crystals, both euhedral and broken. Before running on the Element ICP mass spectrometer, samples were packed into small pieces of niobium tubing with both ends crimped to make a packet. Samples were run on the helium line, and then dissolved in HNO_3 and run on the mass spectrometer. U, Th and He content were measured at the UCSC Thermochronology lab and ages calculated with the help of Dr. Jeremy Hourigan.

IV. Determining Erosion Rate

The cooling ages from Methods III cannot be fully understood without understanding the following: which is the appropriate mean, the mean of the cooling ages or the mean of the inverse cooling ages? In dealing with a ratio, it is important that random samples are taken with respect to the quantity in the numerator (Bernet et al., 2009). This is because the denominator of the ratio can be thought of as a constant interval and so you want to sample with respect to the variable that changes, the numerator.

In measuring erosion rates in the Andes, our technique encompasses a large drainage basin that likely contains smaller regions of different rates of erosion. We want to sample such that we measure the average by area. If something is eroding fast, it would produce more detritus than a slower-eroding

area, bias the sample, and thus we would want to down-weight it. Therefore, instead of erosion rate, we use the inverse erosion rate, called the retention rate. We average the reciprocal of the erosion rate, which is proportional to the average lag time (Fig. 6), to estimate a basin-wide average erosion rate.

Results

Sample Name	Northing	Easting	Elev. (m)	Deposit	Deposit Age	Age (Ma)
LBA-K29	4837150	344133	437	Fenix	15.6±1.1 ka	7.27
LBA-K47	4816450	293941	1457	Mercer	7 to 5 Ma	22.83
LBA-K08	4811623	368316	620	Telken	760±14 to 984±35 ka	7.75
LBA-K17	4811631	368057	632	Telken	760±14 to 984±35 ka	5.25
LBA-N09	4811582	368175	641	Telken	760±14 to 984±35 ka	7.49
LBA-K02	4811435	368353	634	Telken	760±14 to 984±35 ka	6.00
LBA-K10	4811639	368306	620	Telken	760±14 to 984±35 ka	6.47
LBA-K07	4811474	368445	628	Telken	760±14 to 984±35 ka	5.36
LBA-P11	4811468	368153	631	Telken	760±14 to 984±35 ka	3.87
LBA-K21	4811612	368136	637	Telken	760±14 to 984±35 ka	5.17
LBA-N04	4811549	368399		Telken	760±14 to 984±35 ka	4.18
LBA-N08	4811355	368184	655	Telken	760±14 to 984±35 ka	5.34
LBA-K15	4811425	368218	638	Telken	760±14 to 984±35 ka	6.78
LBA-K38	4816618	294008	1472	Mercer	7 to 5 Ma	37.66
LBA-K44	4816308	293928	1465	Mercer	7 to 5 Ma	17.68
LBA-K01	4811448	368298	636	Telken	760±14 to 984±35 ka	--
LBA-K04	4811441	368381	632	Telken	760±14 to 984±35 ka	6.05
LBA-K20	4811610	368141	635	Telken	760±14 to 984±35 ka	5.34
LBA-K24	4837501	344099		Fenix	15.6±1.1 ka	5.11
LBA-K26	4837308	344112	450	Fenix	15.6±1.1 ka	9.14

Table 1: Sample names, locations, and cooling ages for apatite grains from 20 granite cobbles. Ages by C. Willett, Ma and Hourigan.

The depositional ages of these moraines are known and the simple difference between the cooling age and depositional age provides an estimate for the lag time, the elapsed time from crystallization to exhumation to the surface.

The plot below shows the data from Table 1, along with diagonal lines of constant lag time.

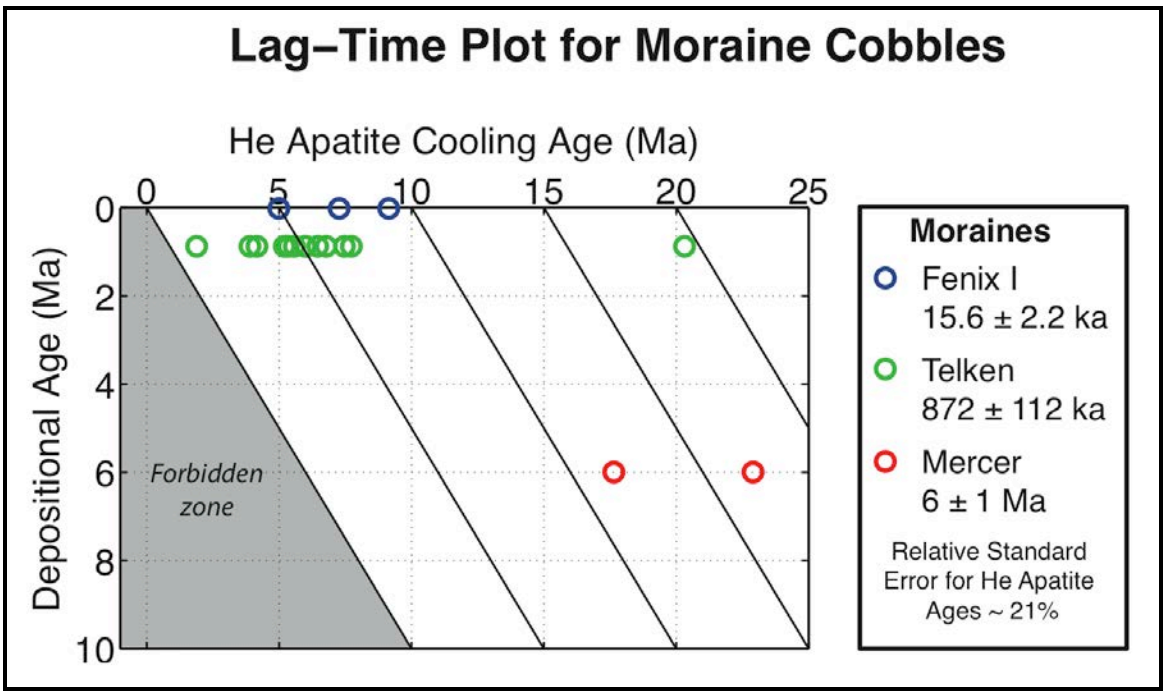

Figure 5: Weighted averages of apatite (AHe) cooling ages are plotted against depositional age. The direct comparison of the points to parallel lines of constant lag time shows that the lag time associated with exhumation has decreased over the past 20 Ma, corresponding to an acceleration in erosion rates. See Table 2 and Figure 6 for determination of erosion rates. Figure by Brandon and C. Willett.

Each of the three sets of ages, one for each deposit, is averaged to calculate a mean lag time, shown in Table 2. These lag times are used below to determine time-averaged erosion rates.

Deposit name	Mean lag time (Ma)
Fenix	7.1
Telken	5.5
Mercer	20.0

Table 2: Mean lag time for each deposit.

Next, I use an age2edot plot to convert the average lag times into average erosion rates (Fig. 6).

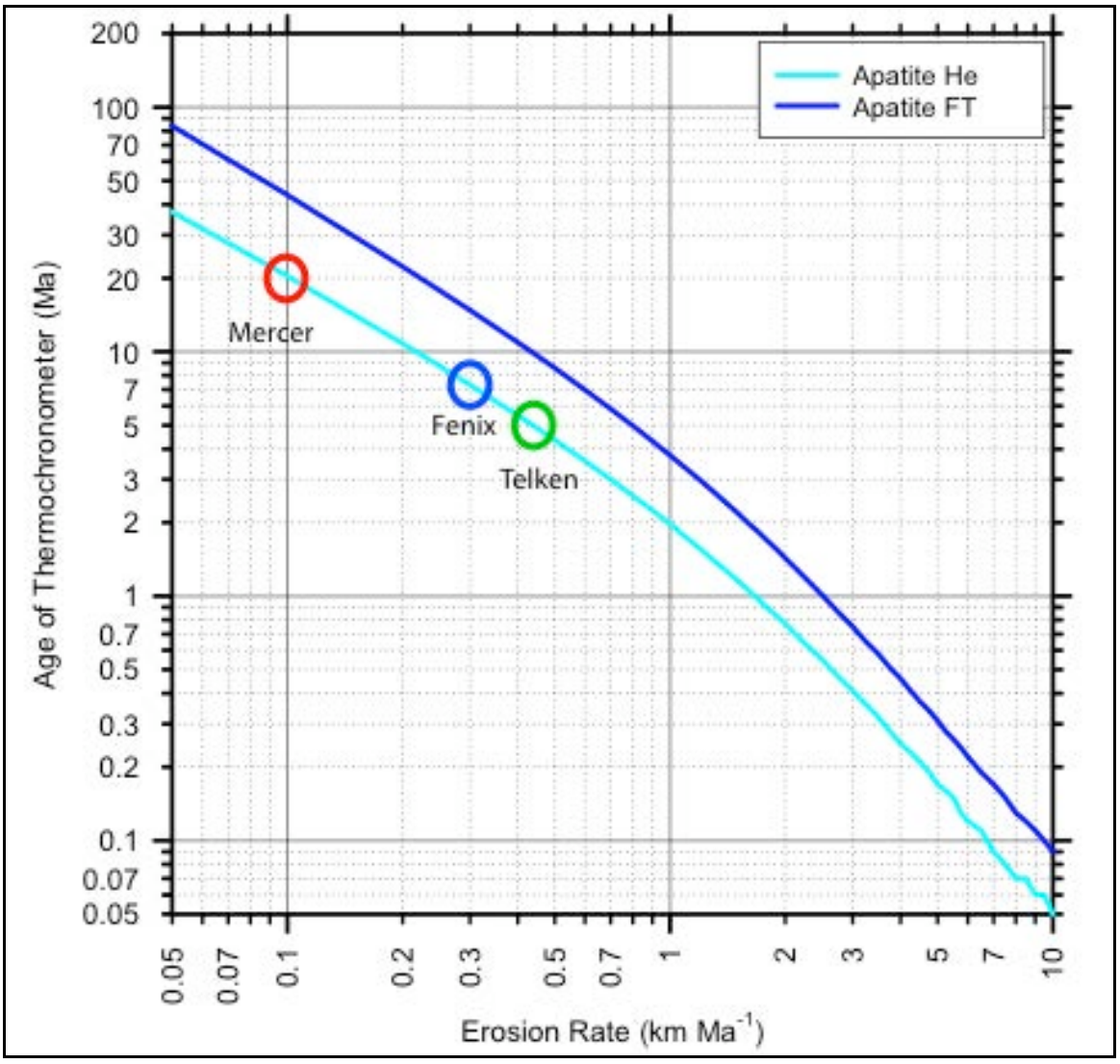

Figure 6: This plot correlates the age of the thermochronometer to the erosion rate, on a logarithmic scale. The plot shows that the measured lag times correlate to erosion rates of 0.1 mm yr^{-1}, 0.3 mm yr^{-1} and 0.45 mm yr^{-1}. (Modified from Reiners and Brandon, 2006)

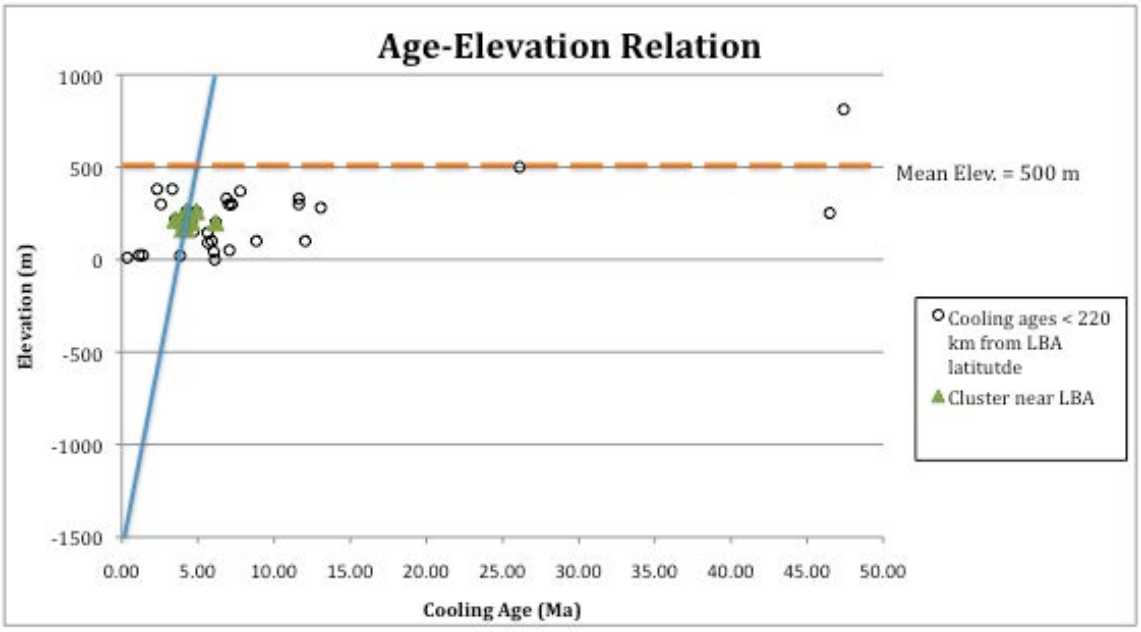

Figure 7: Graph of age-elevation data for bedrock ages from the region. Data are AHe cooling ages from Stuart Thomson (see Appendix). The cooling age is the time of flight from the closure isotherm depth to the mean elevation of the region. Figure by C. Willett.

In an effort to put the cooling ages into context, I refer to Stuart Thomson's Bedrock AHe dataset. I plot the elevation versus cooling age for samples within about 2° latitude from Lago Buenos Aires (Fig. 7). Looking at this plot, we see that virtually all the bedrock samples are taken from valleys, below the region's mean elevation of 500 m. The green triangles in Figure 7 are the points from a linear sampling string just northeast of the North Patagonian Ice Sheet (see Fig. 8). These points have an average cooling age of about 5 Ma. Multiplying cooling age by erosion rate gives closure depth. Erosion rate is from Figure 6.

$$(5\ \text{Ma})*(400\ \text{m Myr}^{-1}) = 2000\ \text{m below the mean elevation,}$$
$$= 1500\ \text{m below sea level, shown in Fig 7}$$

A line assuming simple and constant exhumation is drawn in blue. If erosion rates were continuous over the past 20 million years, one would expect

the ages to fall on this line. The scatter in the plot indicates that erosion rates are not constant. Points to right of the line have had erosion rates that are lower.

We can use this blue line to infer what ages we would expect to get if we could sample at higher elevations in the region. High elevation bedrock sampling is difficult because of snow cover and dangerous climbing. Following the blue line, we see that it meets the mean elevation line at an age of about 6 Ma. Using Figure 6 once more, this cooling age corresponds to an erosion rate of about 300 m Myr^{-1}. The bedrock ages imply that erosion rate had varied over time and there was a significant signal for an erosion rate of 0.3 km Myr^{-1}, which matches our data very well.

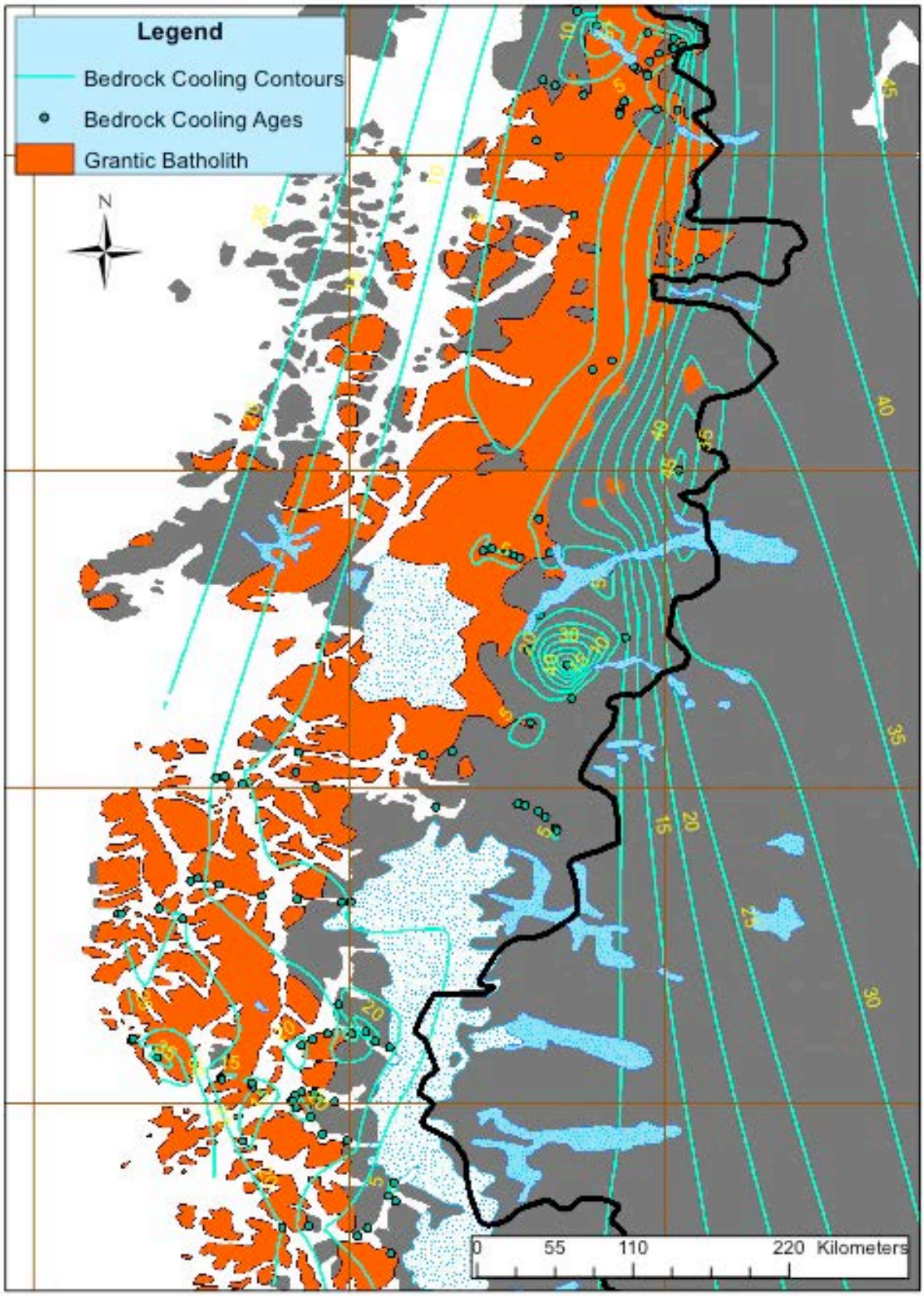

Figure 8: This map shows the batholith in red, the modern ice sheets in blue and white stipples and bedrock cooling age contours. Figure by C. Willett.

Figures 7 and 8 show that rock from the source area is younger than about 10 Ma. However, based on the age-elevation relationship derived in the discussion of Figure 7, we know that bedrock at the summits in the region will be older. Samples of higher elevation could have cooling ages over 10 Ma.

This plot also shows that cobbles from the Mercer deposit would have to be sourced from further to the west because that is where the bedrock ages are sufficiently old, given the erosion rates. As results from the rest of the apatite and zircon dates come through, the understanding of cobble sourcing within the batholith will become clearer.

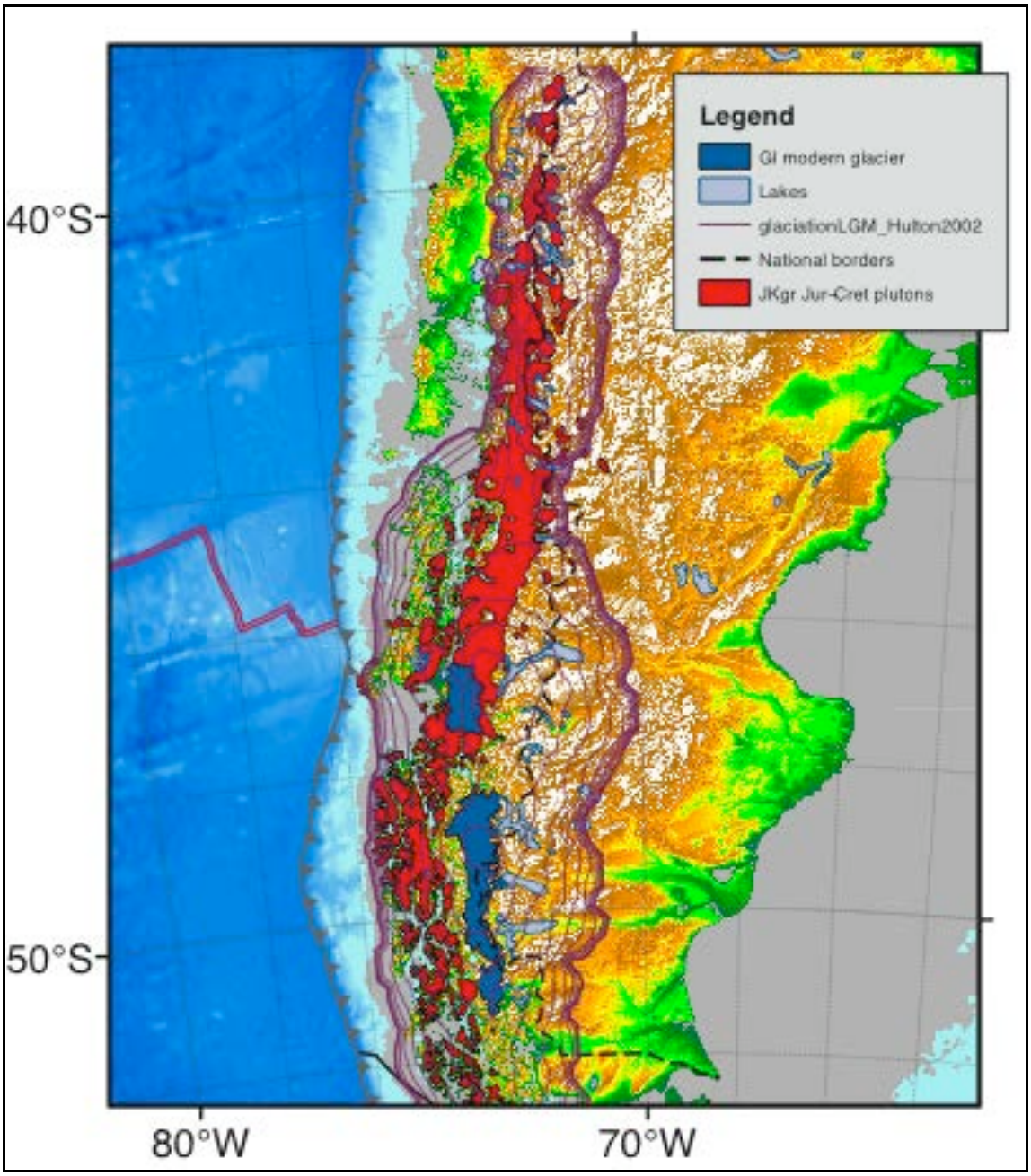

Figure 9: Hulton ice model overlain on a topographic map of the region. Lago Buenos Aires is in the middle and it is clear that the large ice sheet is flowing out through the valley and into and beyond Lago Buenos Aires. Note that central axis of the ice sheet moves east when the ice sheet is bigger. Figure by C. Willett and Brandon.

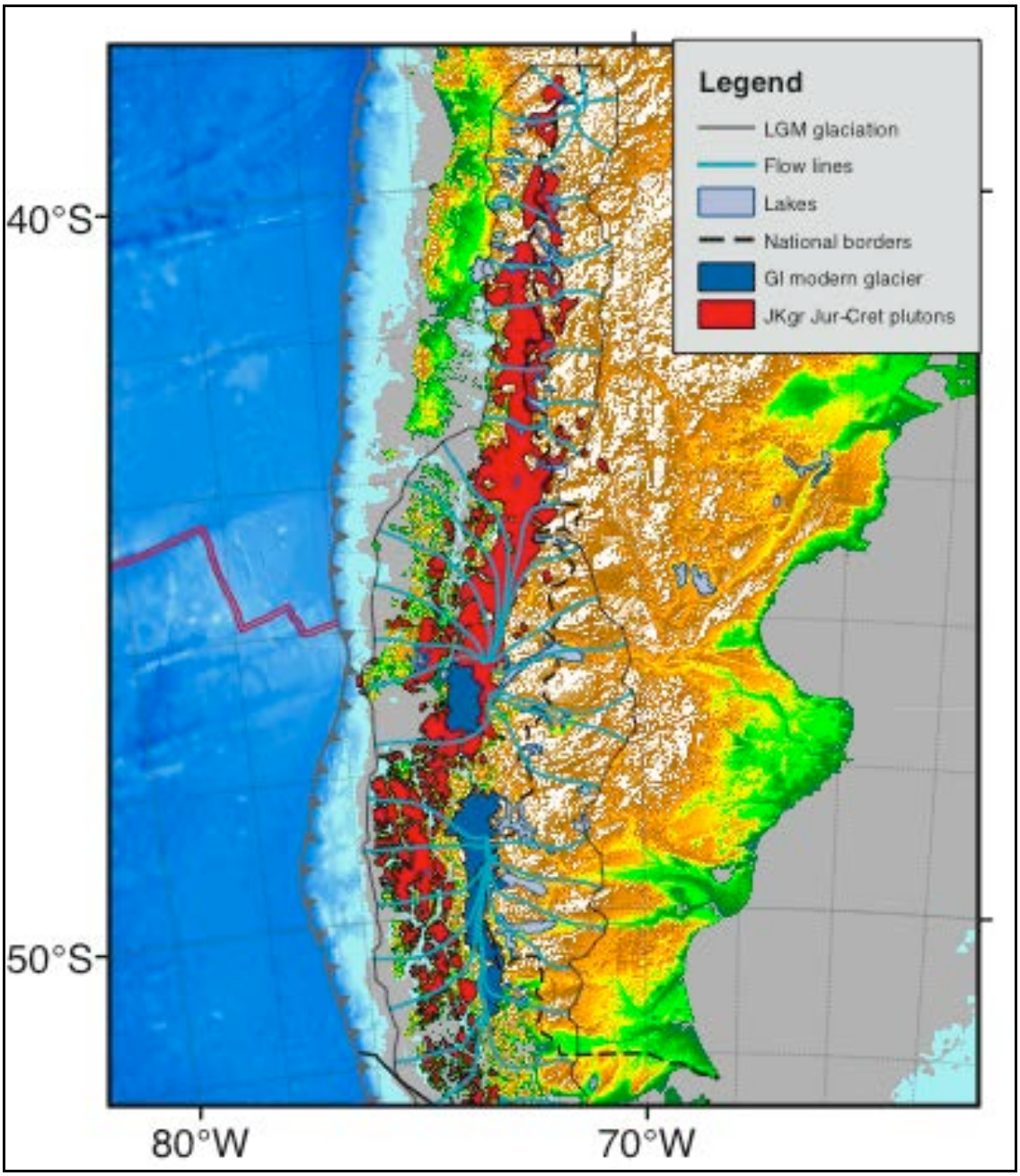

Figure 10: This map shows the flow lines associated with the ice sheet of the Last Glacial Maximum, overlaying a relief map of the region with the Jurassic-Cretaceous granitic plutons and modern ice fields shown. Figure by C. Willett and Brandon.

Discussion

We use the average cooling ages from the source region to determine a basin-wide erosion rate. This approach enables us to look farther in geologic history than looking at bedrock ages alone, though both sets of ages are valuable. We generate an unbiased estimate for the regional-scale erosion in the high Andes. The project reports a preliminary dataset of AHe cooling ages from 20 of 125 samples from two glacial moraines and one till. Preliminary results indicate that the erosion rate in Patagonia has accelerated over the past 20 Ma. Shown in Figure 5, erosion rates have increased from 0.1 to 0.3 and 0.45 mm yr^{-1}, assuming that our sparse ages are representative. While the data are still quite preliminary, they point to a weak buzz saw, explained below. Additionally, study of Hulton's ice model indicates that an ice cap is needed for transport.

I. Weak Buzz Saw

A few unanswered questions make it difficult to draw hard and fast conclusions. First, the idea that glaciation began 6 million years ago is based only on the existence of the Mercer till. Older moraines, were they ever present, may have been obliterated by farther advancing ice sheets or sub-aerially eroded away. Preservation potential to the east of Andes is good but certainly not perfect over timescales of tens of millions of years or more. Glaciation, whether starting 6 Ma or earlier, still began well before the Plio-Pleistocene cooling.

Another issue is the fact that the initial height of the mountain belt is not known, although some estimate it to be a few kilometers (Thomson, 2010). As a

simple test to see if erosion rate is fast enough to erode material, imagine the glaciers eroding an inactive mountain belt. That is, isostatic rebound is the only source of belt uplift. If the glacial buzz saw were to erode an isostatic mountain belt, every 1 km of erosion would be compensated by 0.8 km of isostatic rebound. This ratio is determined by the normalized difference between the crustal density and the density of the asthenospheric mantle:

$$(\rho_{AM} - \rho_C)/\rho_C = (3300 \text{ kg m}^{-3} – 2750 \text{ kg m}^{-3})/(2750 \text{ kg m}^{-3}) = 0.2$$

Therefore, an erosion rate of 0.3 km Ma^{-1} would erode 300 m and experience 240 m of uplift in 1 millions years, resulting in a net lowering of only 60 meters. Even if this process goes on for ten million years, the erosion rate is simply not high enough to create the modern topography.

Due to their closeness in age, we expect the LGM moraine to have similar numbers to bedrock. The preliminary Fenix data matches well with bedrock ages from Thomson et al. 2010, but the data from the 6 Ma Mercer deposit gives a slower erosion rate: we don’t have much of a buzz saw. That is, glaciers don’t seem to be very erosive in this setting over these timescales. Investigation of bedrock cooling age data shows that our conclusions about the erosion rates in the basin are sound. The dating of zircon and apatite grains from the remaining cobbles is in progress. These data will afford a clearer understanding of the relationship between glacial extent and erosion rates in the Patagonian Andes.

II. Icecap needed for transport

Though the thermochronometric data indicate that the buzz saw is weak in the Patagonian Andes, we have determined that the range of glacial transport was once much greater than it is today. That is, glaciation was sufficiently extensive to transport granites sourced from the west side of the modern continental divide to the east near Lago Buenos Aires. As shown in Figure 9, the central axis of the ice sheet – the 'ice divide' – at its greatest extent is east of the ice divide today. Figure 10 shows the streamlines calculated for the ice sheet, showing a steepest gradient path from the batholith to the Lago Buenos Aires deposits. The impressive extent and power of these glaciations indicate that, though the glacial buzz saw may be weak, glaciers in the form of an icecap have played crucial role in sculpting the landscape of southern Chile and Argentina. The icecap is the only feasible way to transport material between the two modern countries and the multiple deposits show that icecaps have been present in the region multiple times in the past 10 Ma.

Summary

Glacial erosion has influenced the southern Andes since before the start of the Pleistocene. Erosion rates have accelerated from 0.1 to 0.45 mm yr^{-1} since 6 Ma, but this preliminary dataset points to only a weak glacial buzz saw. Nonetheless, granitic rocks from the Patagonian batholith were glacially transported across the modern continental divide, showing that glaciations from the Plio-Pleistocene and earlier were icecaps and sufficiently extensive to transport material in ways that are not feasible given the modern topography.

Future Work

The work on this project is ongoing. First, apatite grains from the remaining 100 or so samples from the original sampling set are picked, packed and ready to be dated at UCSC. Completing this dataset will allow for the calculation of a more accurate erosion rate and give a better idea of the age distribution of the cobbles within a deposit.

In March 2011, Keith Ma, Elizabeth Brown and I traveled to the research area and collected 53 addition granite cobbles: 10 from Telken V, 10 from Mercer, and 33 from a new sampling location, here called Guivel, after another paper's first author. The Guivel deposit is similar to the Mercer in that it is a glacial till that lies just below the top of the Meseta Buenos Aires, bracketed by two basalt flows; in this case, the bracketing ages are 3.44 ± 0.11 Ma and 3.64 ± 0.11 Ma (Guivel et al., 2006). See Appendix Figures A5 and A6 for Guivel site. Adding more samples to the Telken and Mercer datasets will reduce error

and generate more concrete numbers. Sampling the Guivel deposit enables a reduction in error and a higher resolution understanding of the erosional history in the area by giving a sampling site dated to between 1 and 6 Ma.

As Keith works towards his Doctorate and Mark Brandon continues work with the SALSA group, we will continue to work towards a better understanding of the growth of the Andes from a wide variety of resources and specialists.

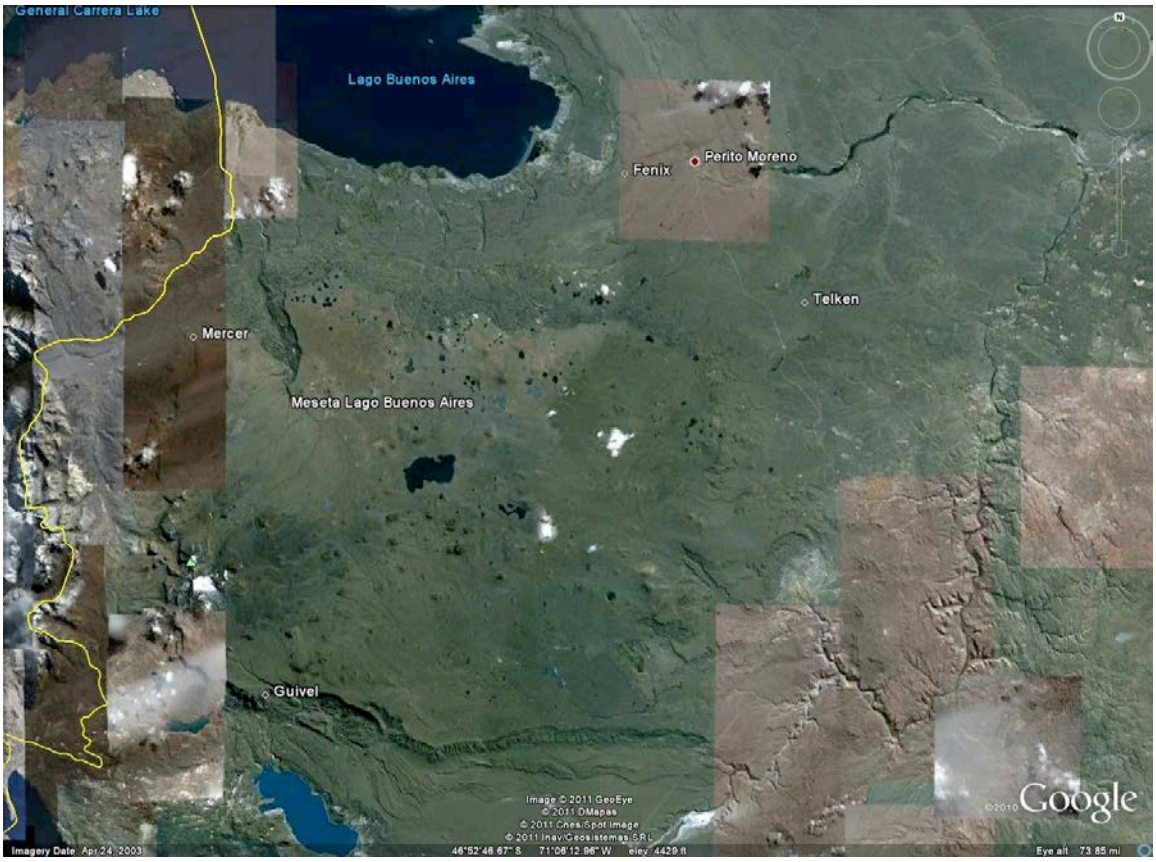

Figure 11: Shows the sampling locations including the new Guivel site on the southern rim of the Meseta Lago Buenos Aires. Created with Google Earth.

Acknowledgements

This work was supported by the Yale College Dean's Research Fellowship in the Sciences**,** the Karen L. Von Damm '77 Undergraduate Research Fellowship in Geology & Geophysics and the Ezra Stiles Senior Mellon Forum Grant**.** Many thanks to Mark Brandon, Jeremy Hourigan, Keith Ma, the Yale Department of Geology & Geophysics and the American Geophysical Union.

References Cited

Bernet, M., M. Brandon, J. Garver, M. L . Balestieri, B. Ventura and M. Zattinz, (2009). Exhuming the Alps through time: clues from detrital zircon fission-track thermochronology. *Basin Research*, **10**.

Brandon, Mark, (2009). Long-term glacial erosion in the Patagonian Andes: Is there a "glacial buzz saw"? Powerpoint presentation. Contact Brandon for reference.

Gregory-Wodzicki, Kathryn M., (2000). Uplift history of the Central and northern Andes: A review. *GSA Bulletin*, **112**, 1091-1105.

Guivel, Christele, D. Morata, E. Pelleter, F. Espinoza, R.C. Maury, Y. Lagabrielle, M. Polvé, H. Bellon, J. Cotten, M. Benoit, M. Suárez and R. de la Cruz (2006). Miocene to Late Quaternary Patagonian basalts (46–47 °S): geochronometric and geochemical evidence for slab tearing due to active spreading ridge subduction, *Journal of Volcanology and Geothermal Research* **149**, pp. 346–370.

Hallet, B., L. Hunter, and J. Bogen (1996), Rates of erosion and sediment evacuation by glaciers: A review of field data and their implications, *Global Planet. Change, **12***, 213-235.

Hubbard, A., Hein, A.S., Kaplan, M.R., Hulton, N.R.J. and Glasser, N., (2005). A modelling reconstruction of the late glacial maximum ice sheet and its deglaciation in the vicinity of the Northern Patagonian Icefield, South America *Geogr. Ann*., **87** A (2): 375–391.

Hulton, N.R.J., R.S. Purves, R.D. McCulloch, D.E. Sugden, M.J. Bentley (2002). The Last Glacial Maximum and deglaciation in southern South America. *Quaternary Science Reviews* **21,** 233–241.

Kaplan, Michael, Robert Ackert, Jr., Brad Singer, Daniel Douglass, Mark Kurtz, (2004). Comsogenic nuclide chronology of millennial-scale glacial advances during O-isotope state 2 in Patagonia. *GSA Bulletin*, **116**, 308-321.

Kaplan, Michael, Andrew S. Hein, Alun Hubbard and Simon M. Lax (2009). Can glacial erosion limit the extent of glaciation? *Geomorphology* **103**, 172–179.

Lagabrielle, Yves, Bruno Scalabrino, Manuel Suárez, Jean-François Ritz (2010). Mio-Pliocene glaciations of Central Patagonia: New evidence and tectonic implications. *Andean Geology*, **37** (2), 276-299.

Lagabrielle, Yves, Manuel Suárez, Eduardo Rossello, Gérard Hérail, Joseph Martinod, Marc Régnier, Rita de la Cruz (2004). Neogene to Quaternary tectonic evolution of the Patagonian Andes at the latitude of the Chile Triple Junction. *Tectonophysics,* **385**, 211-241.

Mercer, J. H. and J. F. Sutter, (1982). Late Miocene-earliest Pliocene glaciation in southern Argentina: implications for global ice sheet history. *Palaeogeography, Palaeoclimatology, Palaeocology*, **38**, 185-206.

Montgomery, D. R., G. Balco, and S. D. Willett (2001), Climate, tectonics, and the morphology of the Andes, *Geology,* **29** (7), 579-582.
Image for Figure 2 at:
http://geology.geoscienceworld.org/content/vol29/issue7/images/large/i0091-7613-29-7-579-f01.jpeg

Reiners, Peter W. and Mark T. Brandon, (2006). Using thermochronology to understand orogenic erosion. *Annu. Review of Earth Planet. Sci.* **34**, 419-466.

Singer, Brad S., Robert P. Ackert, Jr., Herve Guillou, (2004). 40Ar/39Ar and K-Ar chronology of Pleistocene glaciations in Patagonia. *GSA Bulletin*, **116**, 434-450.

Thomson, Stuart N, Mark T. Brandon, Jonathan H. Tomkin, Peter W. Reiners, Cristián Vásquez, (2010). Glaciation as a destructive and constructive control on mountain building. *Nature* **467**, 313-317.

Thomson, Stuart N. (2002). Late Cenozoic geomorphic and tectonic evolution of the Patagonian Andes between latitudes 42°S and 46°S: An appraisal based on fission-track results from the transpressional intra-arc Liquine-Ofqui fault zone. *GSA Bulletin*; **114**; no. 9; p. 1159–1173.

Appendix

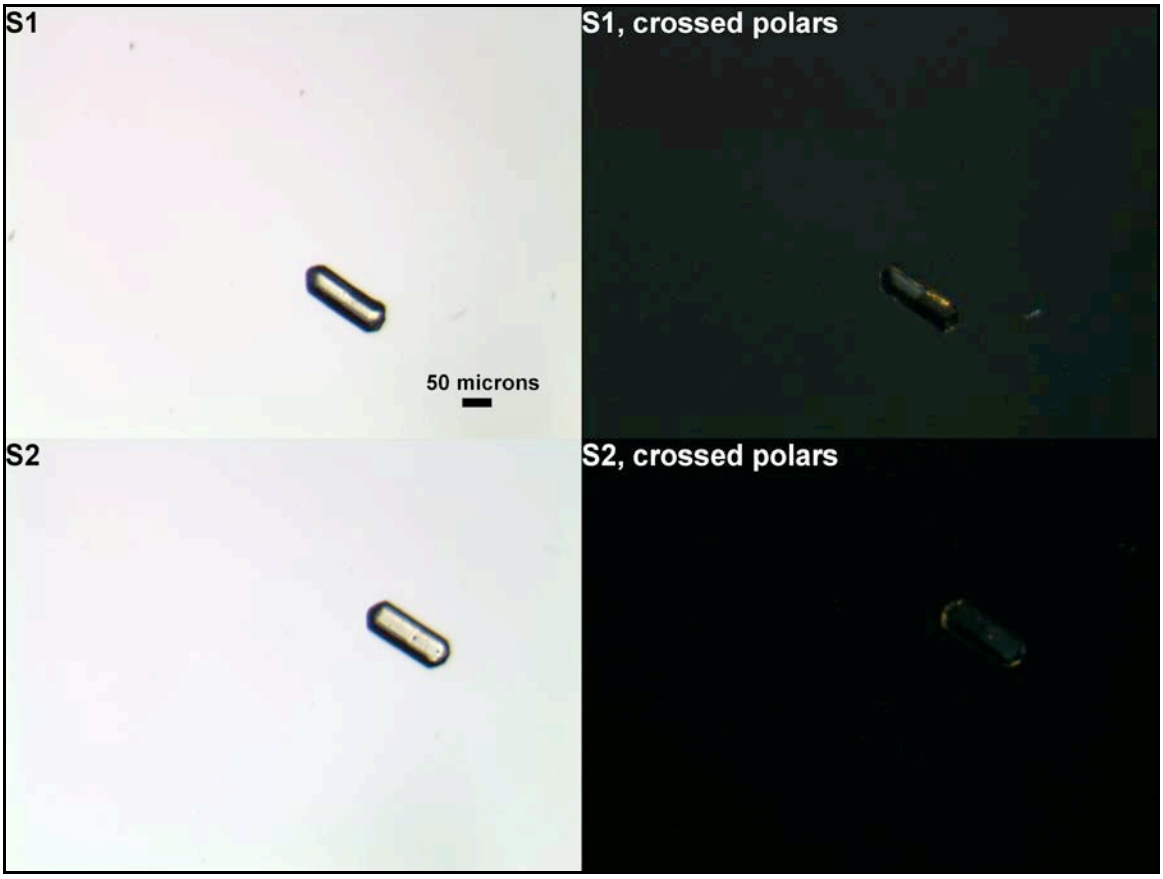

Appendix Figure A1: An apatite crystal from sample with few inclusions and nicely formed ends. Grain is about 70 microns across.

Appendix Figure A2: Many crystals had fractured ends or inclusions, but were chosen because they were the best the sample contained.

Sampling Sites:

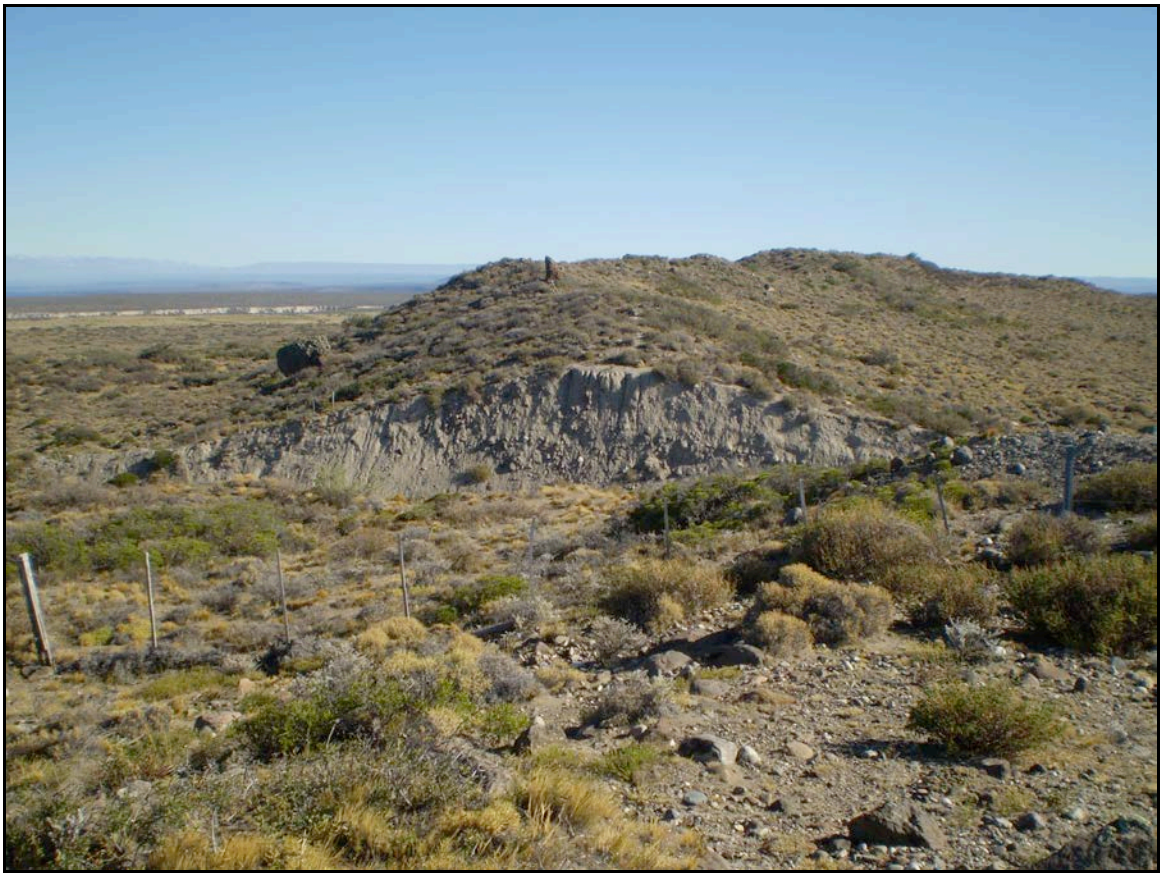

Appendix Figure A3: View of Fenix moraine taken from atop the moraine and looking towards Ruta 43 road cut (facing north). Fence for scale. Photo taken by C. Willett, March 5, 2011.

Appendix Figure A4: The non-descript but gently rolling foreground is the Telken V moraine deposit. Photo taken to the east. Chelsea Willett in orange jacket for scale. Photo taken by Keith Ma, March 5, 2011.

Appendix Figure A5: View of Mercer outcrop, just below the top of Meseta Lago Buenos Aires. Cliffs of basalt flows at top with glacial till at camera level (facing southwest). Photo taken by C. Willett, March 6, 2011.

Appendix Figure A6: View of bracketed Guivel Till, taken from ~1 km away. Cliffs are basalt flows with angled deposits of till and scree between them. Photo faces the northeast. Photo taken by C. Willett, March 9, 2011.

Appendix Figure A7: View of Guivel Till at eye level. Cliff basalts flows alternate with angled tills. Canyon in background is fluvial Rio Correntoso canyon. Photo facing northeast. Photo taken by C. Willett, March 9, 2011.

Thomson Dataset (values used for Fig. 7 in yellow)

Lat	Lon	Elev	AHe Age	AHe Err
-55.9759	-67.2893	0	42.43	3.74
-53.5700	-72.4032	0	7.66	0.43
-53.5700	-72.4032	0	10.69	1.83
-53.5700	-72.4032	0	9.75	1.16
-53.5327	-72.3527	0	6.29	0.73
-53.5327	-72.3527	0	8.17	1.28
-53.5327	-72.3527	0	10.61	1.18
-53.5093	-72.5588	0	12.14	0.58
-53.5093	-72.5588	0	14.52	0.77
-53.4297	-72.9127	0	11.17	0.62
-53.4297	-72.9127	0	15.30	3.08
-53.4205	-72.5938	0	11.94	0.65
-53.3450	-73.1035	0	7.71	0.57
-53.3450	-73.1035	0	12.65	0.42
-53.3450	-73.1035	0	20.03	2.07
-53.1567	-73.2935	0	10.09	0.25
-52.9752	-72.9528	0	7.01	0.25
-52.7265	-73.3678	0	7.40	0.61
-52.7265	-73.3678	0	9.35	0.33
-52.4250	-73.7497	0	11.13	1.88
-52.4175	-73.7598	0	10.86	0.91
-52.4175	-73.7598	0	11.30	1.08
-52.4175	-73.7598	0	10.63	0.36
-52.4110	-73.7437	0	17.00	1.30
-51.8598	-73.8093	1	13.58	0.31
-51.8598	-73.8093	1	9.49	0.36
-50.9566	-73.7317	1	13.39	0.23
-50.9566	-73.7317	1	9.97	6.69
-50.8458	-73.9458	0	11.41	1.00
-50.8458	-73.9458	0	7.68	0.17
-50.7933	-73.8808	0	8.45	0.20
-50.7883	-74.4238	0	14.40	1.29
-50.7883	-74.4238	0	20.15	0.61
-50.7817	-74.2575	0	16.43	0.92
-50.7817	-74.2575	0	10.79	0.24
-50.6236	-73.7019	1	4.90	0.10
-50.6236	-73.7019	1	5.87	1.06
-50.5892	-73.7520	0	5.03	0.20
-50.5088	-73.7158	0	6.64	0.43
-50.5088	-73.7158	0	3.92	0.09
-50.2429	-74.6715	1	13.77	0.32
-50.2429	-74.6715	1	14.24	0.37
-50.2382	-74.0100	0	11.78	0.46
-50.2382	-74.0100	0	17.74	0.52
-50.1990	-74.1668	0	22.88	3.35
-50.1990	-74.1668	0	17.39	0.57
-50.0890	-74.2427	0	17.88	3.70

-50.0890	-74.2427	0	29.23	1.06
-50.0890	-74.2427	0	21.06	1.75
-50.0300	-74.3328	0	18.67	1.00
-50.0300	-74.3328	0	22.00	0.61
-49.9959	-74.0922	1	12.08	0.24
-49.9959	-74.0922	1	18.19	0.78
-49.9888	-74.3620	0	15.04	0.60
-49.9888	-74.3620	0	17.49	0.47
-49.9860	-74.3565	0	28.87	2.15
-49.9860	-74.3565	0	15.08	0.57
-49.9735	-74.1852	1	11.67	0.23
-49.9735	-74.1852	1	14.81	0.53
-49.9536	-74.3413	1	16.50	0.31
-49.9536	-74.3413	1	18.46	2.15
-49.9406	-74.2222	1	16.69	0.34
-49.9392	-74.5548	0	15.20	0.75
-49.9392	-74.5548	0	25.19	0.63
-49.9392	-74.5548	0	10.81	0.32
-49.9327	-74.3008	1	20.35	0.55
-49.9327	-74.3008	1	21.02	2.04
-49.8993	-74.6097	0	11.75	0.72
-49.8993	-74.6097	0	16.20	0.48
-49.8765	-74.6158	0	12.22	0.96
-49.8765	-74.6158	0	14.10	0.40
-49.8517	-74.8032	0	13.85	1.57
-49.8517	-74.8032	0	17.92	1.20
-49.8453	-74.8127	0	19.26	1.34
-49.8453	-74.8127	0	13.53	0.83
-49.7135	-75.2120	0	25.01	0.81
-49.7135	-75.2120	0	40.24	1.21
-49.6479	-73.7405	1	23.07	0.58
-49.6479	-73.7405	1	16.09	0.45
-49.6374	-74.3010	1	32.65	0.82
-49.6374	-74.3010	1	22.37	2.12
-49.6116	-73.8333	1	25.53	0.69
-49.6116	-73.8333	1	16.58	1.63
-49.6050	-75.3790	100	34.86	2.18
-49.6050	-75.3790	100	31.88	1.08
-49.5987	-74.2301	1	14.66	0.58
-49.5932	-75.3710	0	25.59	1.75
-49.5932	-75.3710	0	16.77	0.44
-49.5638	-74.1366	1	28.42	0.71
-49.5638	-74.1366	1	22.00	0.67
-49.5632	-73.9821	1	11.18	0.28
-49.5632	-73.9821	1	4.04	0.13
-49.5511	-73.8929	1	27.68	0.73
-49.3764	-74.0633	1	15.27	0.37
-49.3764	-74.0633	1	14.44	0.88
-48.8340	-75.0518	0	21.10	0.98

-48.8340	-75.0518	0	20.26	0.49
-48.8025	-75.4655	0	35.36	2.68
-48.8025	-75.4655	0	17.92	0.44
-48.8018	-75.4427	0	20.46	1.22
-48.8018	-75.4427	0	16.80	0.37
-48.7695	-75.2022	0	24.08	0.52
-48.7695	-75.2022	0	20.05	0.45
-48.7288	-73.9872	0	6.21	0.93
-48.7288	-73.9872	0	6.93	0.17
-48.7278	-74.0458	0	13.19	0.32
-48.7278	-74.0458	0	15.42	0.38
-48.7092	-74.3288	0	11.10	0.55
-48.7092	-74.3288	0	10.61	0.24
-48.6885	-74.5535	0	15.58	0.65
-48.6885	-74.5535	0	10.49	0.66
-48.6167	-74.8240	0	9.86	1.02
-48.6167	-74.8240	0	11.69	0.27
-48.5943	-75.0037	0	18.56	0.49
-48.5943	-75.0037	0	17.98	0.41
-48.5767	-74.9550	0	20.54	1.03
-48.5767	-74.9550	0	16.64	0.39
-48.2767	-72.6818	270	4.83	0.30
-48.2585	-72.6896	263	4.76	0.51
-48.2585	-72.6896	263	5.99	0.40
-48.1894	-72.7571	299	4.79	0.15
-48.1894	-72.7571	299	5.24	0.17
-48.1507	-72.7989	308	8.79	0.29
-48.1507	-72.7989	308	5.57	0.18
-48.1260	-73.4493	0	5.80	0.31
-48.1260	-73.4493	0	5.07	0.19
-48.1165	-72.8837	412	7.08	0.21
-48.1072	-72.9308	118	7.64	0.30
-48.1072	-72.9308	118	6.16	0.16
-48.1038	-72.9268	127	8.74	0.27
-48.0067	-74.2080	0	5.23	0.90
-48.0067	-74.2080	0	6.43	0.15
-47.9780	-74.6737	0	10.28	0.18
-47.9413	-74.8422	0	15.42	0.27
-47.9413	-74.8422	0	16.99	0.44
-47.9413	-74.8422	0	14.90	0.35
-47.9387	-74.8278	0	11.57	0.69
-47.9307	-74.7847	0	11.03	0.21
-47.9050	-74.3355	0	9.18	0.32
-47.9050	-74.3355	0	9.17	0.22
-47.7947	-73.5289	50	7.07	0.25
-47.7777	-74.3182	0	6.10	0.42
-47.7716	-73.3460	42	6.04	0.21
-47.5925	-72.8515	20	3.82	0.06
-47.4363	-72.5880	300	7.05	2.67

-47.4363	-72.5880	300	7.23	0.22
-47.2230	-72.6153	250	46.47	2.04
-47.1292	-72.8644	100	8.83	0.30
-47.1292	-72.8644	100	12.03	2.12
-47.0530	-72.2478	370	7.76	0.17
-46.9065	-72.7892	330	11.62	2.32
-46.9065	-72.7892	330	6.89	0.55
-46.6288	-72.3587	380	3.32	0.25
-46.6288	-72.3587	380	2.32	0.06
-46.5476	-72.9149	260	4.25	0.12
-46.5476	-72.9149	260	4.89	0.13
-46.5330	-72.9575	216	3.93	0.12
-46.5330	-72.9575	216	3.51	0.10
-46.5187	-72.9953	200	6.16	1.03
-46.5187	-72.9953	200	4.59	0.09
-46.5172	-73.0101	166	4.26	0.13
-46.5172	-73.0101	166	3.98	0.12
-46.5162	-72.7292	280	13.08	0.89
-46.5007	-73.1497	151	4.69	0.18
-46.4886	-73.0934	146	5.63	0.31
-46.3007	-72.7980	300	2.57	0.63
-46.3007	-72.7980	300	11.61	0.53
-45.9887	-71.9090	811	47.40	0.82
-45.3535	-72.4572	89	5.65	0.11
-45.2968	-72.3335	100	5.90	1.07
-44.6510	-71.7750	500	26.13	0.45
-44.3723	-72.5737	10	0.36	0.01
-44.0033	-72.6667	25	1.15	0.04
-44.0033	-72.6667	25	1.39	0.05
-43.9017	-72.8133	25	1.28	0.07
-43.9017	-72.8133	25	0.79	0.65
-43.7367	-72.2850	75	2.56	0.11
-43.7367	-72.2850	75	1.37	0.12
-43.7183	-72.2750	75	2.94	0.09
-43.7183	-72.2750	75	2.03	0.07
-43.7083	-71.9167	1500	23.30	0.71
-43.7083	-71.9167	1500	14.70	2.12
-43.7033	-72.0483	1670	4.55	0.17
-43.7033	-72.0483	1670	4.02	1.34
-43.7033	-72.2800	75	1.46	0.04
-43.7033	-72.2800	75	1.53	0.54
-43.6533	-72.2550	1625	2.45	0.08
-43.6533	-72.2550	1625	5.49	0.77
-43.6117	-72.5117	1490	1.84	0.06
-43.6117	-72.5117	1490	2.41	0.34
-43.5533	-72.6950	1350	1.80	0.06
-43.5533	-72.6950	1350	3.95	0.73
-43.5167	-72.7717	1450	2.20	0.07
-43.5167	-72.7717	1450	3.52	0.26

-43.4913	-72.1087	40	3.37	0.49
-43.4913	-72.1087	40	4.94	0.23
-43.4735	-72.1091	147	4.51	0.10
-43.4735	-72.1091	147	2.37	0.06
-43.4500	-72.1717	1650	1.82	0.06
-43.4500	-72.1717	1650	2.38	0.12
-43.4352	-72.1945	50	2.56	0.25
-43.4352	-72.1945	50	5.97	0.20
-43.4352	-72.1945	50	1.48	0.05
-43.3993	-72.0930	100	4.13	0.27
-43.3993	-72.0930	100	5.75	0.18
-43.3492	-72.0365	190	5.18	0.12
-43.3492	-72.0365	190	2.43	0.12
-43.3183	-71.9414	701	4.02	0.39
-43.3183	-71.9414	701	3.09	0.72
-43.3102	-71.9520	613	2.43	0.09
-43.3102	-71.9520	613	2.97	0.09
-43.3033	-71.8850	1700	3.62	0.10
-43.3033	-71.8850	1700	3.79	0.11
-43.2523	-71.9405	421	3.73	0.52
-43.2523	-71.9405	421	3.86	0.24
-43.2183	-72.1033	1725	2.52	0.07
-43.2183	-72.1033	1725	3.04	0.09
-43.1812	-71.7795	300	22.93	0.92
-43.1760	-72.4307	30	19.71	0.63
-43.0817	-72.5550	1275	1.63	0.05
-43.0817	-72.5550	1275	1.55	0.22
-39.9029	-73.4979	30	32.59	1.96
-39.8305	-71.8314	1050	2.18	0.13
-39.7344	-71.6945	750	2.39	0.14
-39.6885	-73.3471	370	23.87	1.43
-39.6466	-71.8134	880	2.26	0.14
-39.4191	-72.7203	90	8.82	0.53
-39.0444	-71.8023	370	0.98	0.06
-38.8524	-71.5969	550	1.42	0.09
-38.8021	-71.2714	1180	12.50	0.75
-38.7366	-71.5537	1870	7.30	0.44
-38.7302	-71.5397	1709	6.84	0.41
-38.7166	-71.6208	984	3.03	0.18
-38.7067	-71.4700	1450	4.39	0.26
-38.6676	-71.3874	1300	4.30	0.26
-38.6559	-71.6014	1490	4.32	0.12
-38.6559	-71.6014	1490	4.60	0.27
-38.6542	-71.6021	1334	5.88	0.18
-38.6542	-71.6021	1334	5.05	0.17
-38.6182	-71.0155	1180	10.99	0.66
-38.5994	-70.8287	2270	48.61	2.92
-38.5994	-70.8287	2270	60.16	3.61